Formation of armenite in the Berisal Complex, Simplon Region, Switzerland

Schweizerische Mineralogische und Petrographische Mitteilungen 83, 243–259, 2003

Formation of armenite in the Berisal Complex, Simplon Region, Switzerland

Callum J. Hetherington[1,*], *Joseph Mullis*[1], *Stefan Graeser*[2] and *Reto Gieré*[3,**]

Abstract

Armenite ($BaCa_2Al_6Si_9O_{30}\cdot 2H_2O$) occurs in an outcrop of leucocratic celsian + margarite + quartz + white mica + zoisite gneiss in the Berisal Complex, Swiss Central Alps. The locality is cut by undeformed, late-stage, Alpine quartz veins. Armenite crystals are found at the interface between quartz veins and leucocratic host rock, and in a narrow zone of re-crystallised wall-rock gneiss running parallel to the veins. The veins are 15–30 cm thick, cut the dominant foliation of the host rock at 90°, and have a sub-parallel orientation to the nearby Simplon Fault Zone and other local features of extension and uplift. The zone of wall-rock alteration extends 30–50 cm from the vein along foliation. In this zone, the whole-rock Ba content decreases as does the modal abundance of armenite along foliation away from the vein. The decrease is mirrored by an increase in the modal quantities of zoisite, celsian, quartz and margarite. A detailed petrographic and microthermometric study of material from the vein-gneiss interface has been made, and a fluid P–T path has been constructed.

Petrographically, eight events are recognisable in the outcrop, all of which postdate the ductile-to-brittle transition, which the rock passed through during exhumation. Associated with these events, eight fluid-inclusion assemblages have been identified that constrain the retrogression of the rocks and allow identification of the processes that were important in the crystallisation of armenite. The chemical components required for armenite formation occur throughout the gneiss outcrop, but armenite has a limited spatial distribution close to the veins. This suggests that the conditions favourable for armenite formation were restricted to the immediate vicinity of the veins. Three groups were identified amongst the eight fluid-inclusion assemblages: the two oldest ones, found in vein-fill quartz, are aqueous with *c.* 24 mol% CO_2 and no salt. The second group, associated with armenite formation, are trapped in younger vein-fill quartz, in fracture planes in quartz and armenite, and in two generations of armenite. These inclusions are CO_2-depleted, water-rich, and contain 3–9 wt% NaCl. The third group is water-rich, and is found in very late vein-fill quartz.

We conclude that regional fracturing events brought about a considerable decrease in P_{fluid} which led to an influx of water-rich, salt-bearing fluids. The changes in fluid chemistry led to formation of armenite by *in-situ* recrystallisation of pre-existing Ba-, Ca- and Al-rich minerals.

Keywords: Armenite, Berisal Complex, Switzerland, fluid inclusions, fluid composition.

1. Introduction

Armenite, $BaCa_2Al_6Si_9O_{30}\cdot 2H_2O$, is a rare double-ring silicate belonging to the milarite group (Forbes et al., 1972). Members of the milarite group, typically found in low-pressure environments, are described with the general formula $^{[6]}A_2{}^{[9]}B_2{}^{[12]}C{}^{[18]}D{}^{[4]}T(2)_3{}^{[4]}T(1)_{12}O_{30}$, where: A = Mg, Ca, Fe, Ti or Zr; B = K, Na, Mg or H_2O; C = K, Na, Ca or Ba; D = □ or H_2O; T(2) = Al, Be, Mg, Fe or Li; and T(1) = Si and Al. No significant quantities of CO_2, OH, or other volatile species have been recorded. Armenite is an atypical member of the milarite group because it has pseudo-hexagonal symmetry rather than pure hexagonal symmetry. Moreover, it is the only member reported to contain H_2O on the D-site (Forbes et al., 1972). The milarite structure can accommodate up to 21

[1] Mineralogisch-Petrographisches Institut, Universität Basel, Bernoullistrasse 30, CH-4056 Basel, Switzerland. <joseph.mullis@unibas.ch>
* Present address: Geologisk Museum, Universitetet i Oslo, PO Box 1172, Blindern NO-0318, Oslo, Norway. <callum.hetherington@nhm.uio.no>
[2] Naturhistorisches Museum, Augustinergasse 2, CH-4001, Basel, Switzerland. <stefan.graeser@unibas.ch> (and Mineralogisch-Petrographisches Institut, Universität Basel, Bernoullistrasse 30, CH-4056 Basel, Switzerland).
[3] Department of Earth and Atmospheric Sciences, Purdue University, 550 Stadium Mall Drive, West Lafayette, IN 47907-2051, USA.
**Present address: Institut für Mineralogie, Petrologie und Geochemie, Universität Freiburg, Albertstrasse 23b, D-79104 Freiburg, Deutschland. <giere@uni-freiburg.de>

0036-7699/03/0083/243

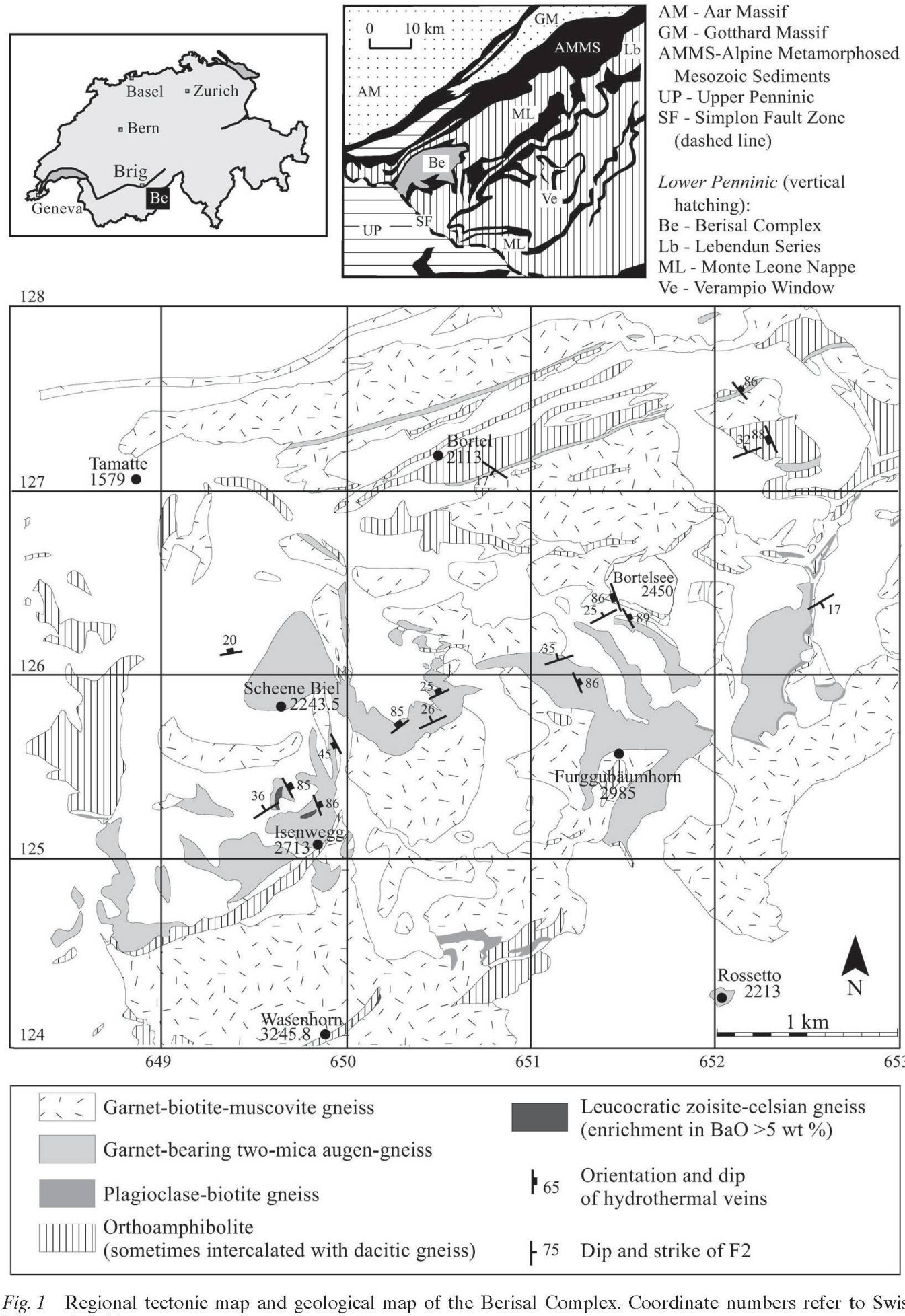

Fig. 1 Regional tectonic map and geological map of the Berisal Complex. Coordinate numbers refer to Swiss kilometric grid.

cations and water molecules per 30 oxygen atoms, but there are few end-members with all sites completely occupied. Armenite does not exhibit full occupancy, as seen when it is presented with the general milarite-group formula, i.e. $Ca_2(H_2O)_2Ba\square Al_3(Si,Al)_{12}O_{30}$. All reported armenites are of nearly end-member composition.

Armenite has been found in various rock types and at several localities (Table 1), which all show evidence of metasomatic/hydrothermal activity. The mineral's occurence in the Berisal Complex in the Simplon area of Switzerland was described previously (Senn, 1989; Graeser, 1993). Recent field work in this area revealed that armenite occurs in a leucocratic gneiss, and that it is closely associated with late Alpine quartz veins (Hetherington, 2001).

The Berisal Complex is the structurally uppermost Penninic unit of the Western Lepontine dome (Fig. 1). It consists of pre-Triassic polymetamorphosed ortho- and paragneisses and a cover of Mesozoic sediments, which were metamorphosed during the Alpine orogeny (Stille, 1980; Frank, 1983). To the southwest, the Complex is bounded by the late Alpine Simplon Fault Zone, a low-angle normal fault which exerted a major tectonic control on uplift and exhumation of the Western Lepontine dome (Merle et al., 1989; Steck and Hunziker, 1994).

In the Berisal Complex, there are several occurrences of rocks with anomalously high barium concentrations (Senn, 1989; Köhn, 1993; Hetherington, 2001), i.e., several thousand parts per million (ppm) Ba (average upper crustal abundance = 700 ppm; Taylor and McLennan, 1981). All localities of Ba enrichment are associated with a large E–W trending body of gneisses, which were interpreted as orthogneisses (Hetherington, 2001). These Ba-enriched rocks are characterised mineralogically by the presence of Ba-rich white micas ± celsian. The highest BaO concentrations (⩾5 wt%) were recorded at two outcrops of zoisite-celsian gneiss (Fig. 1). These outcrops are petrographically and geochemically similar; however one of them is cut by late Alpine quartz veins, and it is only at this locality that armenite occurs. The exclusive occurrence of armenite in close proximity of the late Alpine veins points to an armenite-forming process that was influenced by hydrothermal fluids.

The main goals of this paper are to describe the field relationships, report microscopic observations, and present geochemical and fluid-inclusion data for the various rock types encountered at the armenite outcrop. We then use our observations and data to derive the sequence of events involved in armenite formation, and to assess the

Table 1 Overview of armenite localities from around the world.

Locality	Reference	Host Rock	Associated Minerals
Kongsberg, Armen, Norway	Neumann, 1939	Silver-calcite bearing veins	Po, Ax and Qtz
Rémigny, Quebec, Canada	Pouliot et al., 1984	Prehnitised and epidotised diorites	Thulite, Ab and Pm
Broken Hill, Australia	Mason, 1987	Aplitic gneisses	By and Cln
Tokovian Granite, Pridneprov'ya, USSR	Semenenko et al., 1987	Metasomatised granite	Pl, Prh, Zo, Anl and Ms
Chvaletice, Czech Republic	Zak and Obst, 1989	Basic volcano-sedimentary sequences	Cal, Qtz, Pl, sulphides and Chl
Su Zurfuru, Sardinia, Italy	Balassone et al., 1989	Hornfels and skarns	Qtz, Cal, Chl, Epi and Py
Wasenalp, Simplon, Switzerland	Senn, 1989	Leucocratic gneiss	Cln, Chl, Cal, Ms, Rt and Zo
Coire Loch Kander, Grampian Highlands, Scotland	Fortey et al., 1991	Graphitic schist, sulphide calc-silicate quartz rock	Hy, Chl, Am, Po and Sp

Abbreviations: By—bytownite; Cln—celsian; Hy—hyalophane; Pm—piemontite. All other abbreviations after Kretz (1983).

importance of hydrothermal fluids in the crystallisation of this rare Ba-silicate.

2. Analytical procedures

Whole-rock chemical analyses of the gneisses were made at the Geochemistry Laboratories, University of Basel. Major oxide concentrations were measured on a fused glass bead (20 mm diameter) containing a mixture of 300 mg sample powder and 4700 mg Li-tetraborate. For the analysis of trace elements, a pressed powder pellet (20 mm diameter), mounted in a plexiglas ring, was prepared with 800 or 1000 mg of rock powder and an organic fixing agent. All analyses were obtained with a Siemens SRS3000 Wavelength Dispersive Sequential X-Ray Spectrometer with a Rh end window tube (4 kV). The results were collected and evaluated using the Bruker AXS Spectraplus standardless evaluation programme.

Mineral compositions were determined by electron probe microanalysis (EPMA) using a JEOL JXA-8600 instrument at the University of Basel. The microprobe is equipped with four crystal spectrometers and Voyager software by Noran Instruments. Analyses were made with a focussed electron beam (3 μm diameter), either on a single spot, or scanning over an area of 26 μm^2. The accelerating voltage was 15 kV, the beam current was 10 nA, and the counting times were between 10 and 20 s. The microprobe was calibrated for each element using a range of well characterised natural materials. A ZAF-type correction procedure was used for all data reduction, and all Fe was assumed to be ferrous.

Table 2 Chemical composition of zoisite in leucocratic gneiss (sample SS9793N3), as determined by EPMA.

wt%	Zoisite Representative Analyses		
MgO	<0.01	<0.01	0.01
Al_2O_3	33.8	33.8	33.2
SiO_2	39.9	39.2	39.0
FeO	0.46	1.04	0.75
CaO	23.1	23.1	23.7
MnO	<0.18	<0.18	<0.18
Total	97.4	97.2	96.8
Stoichiometry based on 12.5 oxygens			
Ca	1.88	1.89	1.95
Fe^{2+}	0.03	0.07	0.05
Mn^{2+}	0.00	0.01	0.01
Fe^{3+}	0.00	0.00	0.00
Mn^{3+}	0.00	0.00	0.00
Mg	0.00	0.00	0.00
Al	3.02	3.04	3.01
Si	3.03	2.99	2.99
Σ Cations	7.96	7.99	8.00

Table 3 Chemical composition of celsian in leucocratic gneiss (sample SS9793N3), as determined by EPMA.

wt%	Celsian Representative Analyses		
BaO	38.6	39.2	42.1
K_2O	0.34	0.23	0.15
Al_2O_3	27.4	26.5	28.0
SiO_2	33.8	32.7	33.0
CaO	0.03	0.23	0.01
Na_2O	0.29	0.17	0.25
Total	100.5	99.0	103.5
Stoichiometry based on 8 oxygens			
Ba	0.92	0.96	1.00
K	0.03	0.02	0.01
Na	0.00	0.02	0.00
Ca	0.03	0.02	0.03
Al	1.96	1.95	1.99
Si	2.05	2.04	2.00
Σ Cations	5.00	5.00	5.03

Quartz-armenite bearing veins were sampled so as to take a cross section of a vein and the neighbouring host rock in order to construct a profile of the fluid inclusion assemblages with regard to their spatial orientation. Thick sections of each sample were cut and polished, on both sides, down to a thickness of <0.5 mm using various diamond powder suspensions.

Microthermometric investigations were made on a Chaixmeca heating and cooling stage designed to work in the range of –180 to +600 °C (Poty et al., 1976). The calibration of the apparatus is described in Mullis et al. (1994). The accuracy of measurements is ±0.1 °C between –60 and 40 °C, and ±1 °C for temperatures outside this range. A triple point temperature of –56.6 °C indicates pure CO_2. The melting temperature of CO_2 is very sensitive to the presence of CH_4, H_2S and N_2, especially between –56.6 and –60 °C (Heyen et al., 1982).

In CO_2-bearing aqueous fluids, salinity was derived from the dissociation temperature of clathrate in the presence of pure CO_2 liquid and vapour (Chen, 1972; Bozzo et al., 1973; Diamond, 1992). If the fluid contains small concentrations of other volatiles such as CH_4, H_2S or N_2, clathrate dissociation temperatures rise and lead to underestimated salinities (Diamond, 1994). In gas-absent fluid inclusions, salinity was derived from the ice melting temperature in NaCl-equivalence after Potter et al. (1978).

Liquid-vapour equilibrium temperatures (TH_{CO2}) between 25.5 and 29.5 °C together with

solid-liquid-vapour equilibrium at around –56.6 to –57.2 °C indicates that CO_2 is the main volatile species.

Density was derived from TH_{CO2} (L+V → L), assuming CO_2 to be pure (Angus et al., 1973). The concentration of dissolved CO_2 in aqueous solution was calculated using the Henry's law constant of Drummond (1981) and the CO_2 fugacity at the pressure and temperature of volatile homogenisation or clathrate dissociation.

Bulk homogenisation temperatures were measured for most inclusions. These temperatures were used for the determination of the volume fraction of vapour and liquid phases either for volatile-free aqueous fluid inclusions (Zhang and Frantz, 1987) or for CO_2-bearing inclusions (Schwartz, 1989).

3. Petrographic features of the armenite locality

The armenite-bearing outcrop is located near Isenwegg, to the north of the Wasenhorn (Swiss coordinates 649'600/125'400; 2430 m), and measures approximately 80 by 25 m in size. It consists primarily of leucocratic gneiss exhibiting a penetrative foliation (F2), which strikes E–W, and dips around 36° to the N (Fig. 2). The rock is fine-grained (<0.5 mm) with a syn-kinematic mineral assemblage of celsian + margarite + quartz + Ba-rich white mica + zoisite. Armenite, which is post-kinematic, occurs only in an alteration zone adjacent to and at the edge of late quartz veins, which cross-cut the outcrop.

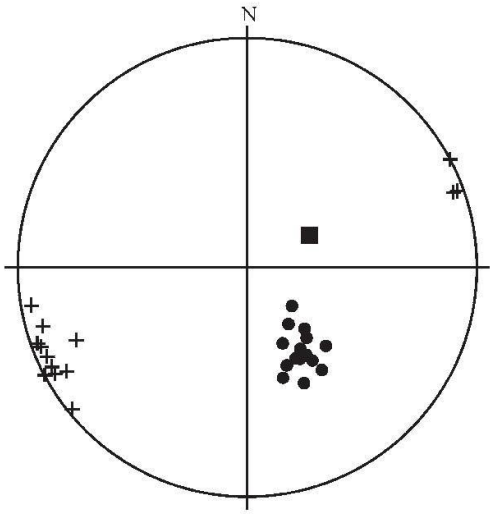

Fig. 2 Equal area stereographic plot (lower hemisphere) showing the relationship between the Simplon Fault Zone, the foliation (F2) of the zoisite-celsian gneiss, and the quartz veins related to armenite. ■: Simplon fault zone (Mancktelow, 1990), ●: foliation of gneiss (n= 16) and +: Late Alpine hydrothermal veins (n= 13).

3.1. Armenite-free rocks

The mineral assemblage in the armenite-free gneiss, outside the alteration zone, is dominated by zoisite (35 vol%), with lower concentrations of celsian (20 vol%), quartz (20 vol%), and margarite (15 vol%). The remaining 10 vol% consist of Ba-rich muscovite or ganterite, a Ba-dominant white mica (Graeser et al., 2003), and accessory apatite and ilmenite. This zoisite-celsian gneiss is very rich in BaO with whole-rock concentrations commonly >5 wt%. Intercalated in this gneiss are small lenses of garnet-chlorite-bearing gneiss and white-mica schist. The garnet-chlorite gneiss contains smaller amounts of zoisite and celsian, and has significantly lower BaO contents than the zoisite-celsian gneiss (Hetherington, 2001). The bands of white-mica schist are rich in BaO (5–8 wt%), and contain quartz and occasionally crystals of zoisite or clinozoisite (Hetherington et al., 2003).

Zoisite, celsian and margarite are all chemically homogenous and have close to pure end-member compositions (Tables 2–4). White mica shows an extensive range of Ba:K ratios (Table 4), but individual crystals are generally homogenous. The observed variation occurs between crystals as well as between individual lenses and bands of zoisite-celsian gneiss.

The syn-kinematic nature of these minerals, their chemical homogeneity and the absence of alteration suggest that the rocks became enriched in Ba prior to, or contemporaneously with, early Alpine metamorphism (Hetherington, 2001; Hetherington et al., 2001).

3.2. Hydrothermal quartz veins

The studied outcrop is cut by a series of late Alpine hydrothermal veins, which are 15–30 cm thick. These nearly vertical veins consist almost exclusively of quartz, exhibit sharp contacts with the host rock, and are not deformed. They are perpendicular to the penetrative main foliation F2 and can be traced for 4–5 m, striking NNW–SSE, i.e., sub-parallel to the nearby Simplon Fault Zone (Figs. 2, 3).

The absence of deformational features and the structural relationships between the quartz veins and the associated armenite mineralisation indicate that both are relatively young, postdating the deformation event that produced F2. Other features of extension and shearing, parallel to the veins, are observed in all lithologies of the Berisal Complex (Hetherington, 2001) and suggest that extensional fracturing occurred on a regional scale.

Table 4 Chemical composition, determined by EPMA, of margarite and Ba-rich muscovite (sample SS9793N3; 2–5 cm from vein-gneiss interface) and ganterite (sample SS9858/3C; 35 cm from the vein-gneiss interface) in leucocratic gneiss.

	Margarite			Ba-rich Muscovite			Ganterite		
wt%	1	2	3	4	5	6	7	8	9
BaO	<0.30	0.62	1.46	7.03	12.5	13.88	16.0	16.9	18.2
K_2O	0.11	0.11	0.11	7.2	5.32	4.5	2.90	2.62	2.05
MgO	0.16	0.13	0.12	1.62	0.70	1.08	0.65	0.67	0.64
Al_2O_3	50.9	51.0	50.0	34.23	37.7	36.23	38.1	37.8	37.4
SiO2	32.1	32.5	31.9	42.35	38.8	38.58	37.1	36.8	34.6
FeO	0.48	0.31	0.37	1.49	1.00	0.69	0.60	0.42	0.65
CaO	10.6	11.0	10.7	0.03	0.04	0.03	<0.06	<0.06	0.01
Na_2O	1.21	1.18	1.02	1.01	1.05	1.48	2.22	2.14	1.73
TiO_2	<0.15	<0.15	0.17	0.71	0.31	0.96	0.43	0.23	0.28
MnO	0.07	0.10	0.10	0.09	<0.02	<0.02	<0.02	0.12	0.06
Total	95.6	96.9	96.0	95.76	97.5	97.43	97.9	97.6	95.7
Stoichiometry based on 22 oxygens									
Ba	0.00	0.03	0.08	0.38	0.69	0.77	0.90	0.96	1.06
K	0.02	0.02	0.02	1.28	0.96	0.82	0.53	0.48	0.39
Na	0.31	0.30	0.26	0.27	0.29	0.41	0.62	0.60	0.50
Ca	1.49	1.53	1.52	0.99	0.01	0.00	0.00	0.00	0.00
Mn	0.01	0.01	0.01	0.01	0.00	0.00	0.00	0.01	0.01
Ti	0.00	0.00	0.02	0.07	0.03	0.10	0.05	0.02	0.03
Mg	0.03	0.03	0.02	1.72	0.15	0.23	0.14	0.14	0.14
Fe	0.05	0.03	0.04	0.17	0.12	0.08	0.07	0.05	0.08
Al_{oct}	4.10	4.06	4.02	3.48	3.74	3.57	3.72	3.73	3.74
Al_{tet}	3.78	3.77	3.77	2.12	2.53	2.51	2.70	2.69	2.84
Si	4.22	4.23	4.23	5.88	5.47	5.49	5.30	5.31	5.16
Σ Cations	14.01	14.01	14.00	14.01	13.98	13.98	14.01	14.00	13.96

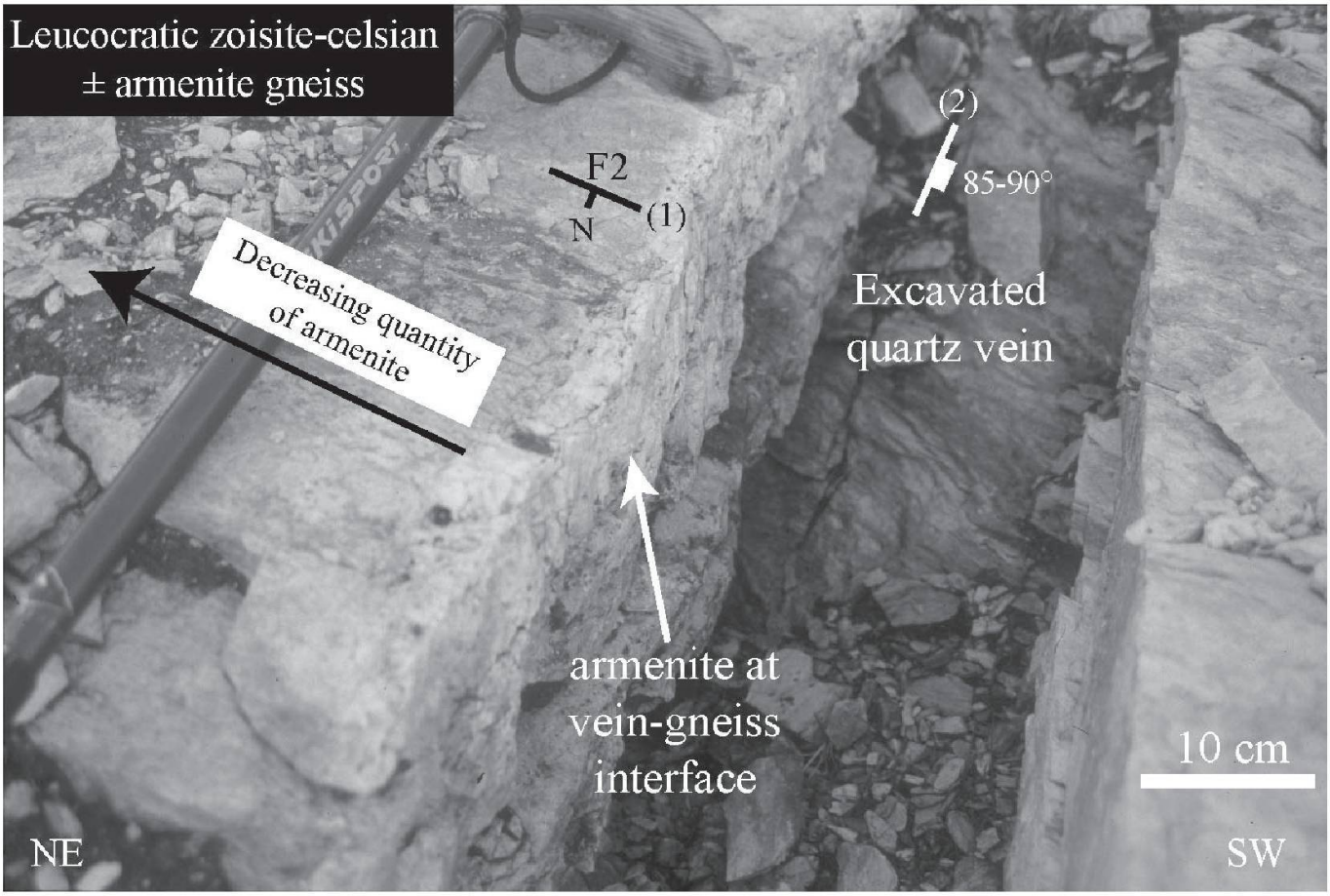

Fig. 3 Photograph of excavated armenite-related late Alpine quartz vein. (1) Dip and strike of penetrative foliation (F2) in the gneiss. (2) Orientation of the late Alpine quartz vein.

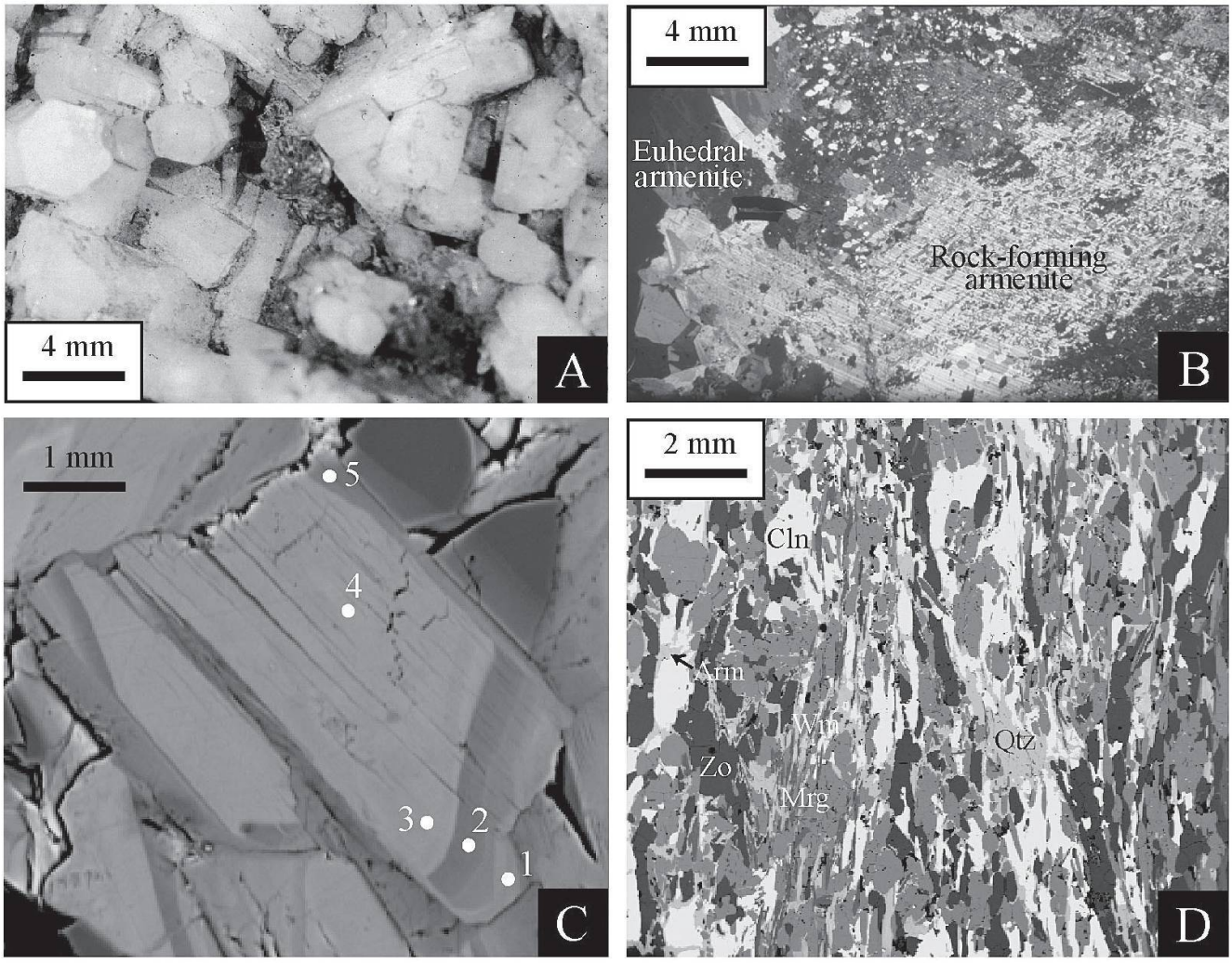

Fig. 4 (A) Randomly oriented euhedral armenite at the vein-gneiss interface. (B) Micrograph of zoisite-celsian gneiss next to the quartz vein with mineral inclusion-bearing rock-forming armenite and inclusion-free euhedral armenite. (C) Back-scattered electron image of a chemically zoned Ba-rich white mica (numbers refer to analyses in Table 6). (D) Back-scattered electron image of armenite-bearing zoisite-celsian gneiss 40 cm from late Alpine quartz vein. Abbreviations: Arm – armenite, Cln – celsian, Wm – White mica. All other abbreviations after Kretz (1983).

3.3. Armenite-bearing rocks

Armenite is only found in close proximity to the late Alpine hydrothermal quartz veins, and occurs in two forms: (1) as euhedral crystals, up to 45 × 20 mm in size, at the interface between veins and zoisite-celsian gneiss; and (2) as a secondary mineral replacing the Alpine mineral assemblage in a narrow zone of altered gneiss directly adjacent to the veins (Fig. 3). In this zone, hydrothermal fluids have greatly altered both fabric and mineral content of the leucocratic gneiss. One of the most notable alteration features is the presence of small cavities, a few mm in diameter, which are more common close to the vein-gneiss interface. Like the quartz veins, neither type of armenite is deformed and thus, both the veins and the armenite crystals may be classified as post-kinematic. The idioblastic armenite crystals at the vein-gneiss interface have a milky-white colour, occur in a random orientation, and contain no mineral inclusions (Figs. 4A, B).

The armenite-bearing zone of altered gneiss is 30–50 cm wide, and its boundary towards the non-altered zoisite-celsian gneiss is more or less parallel to the veins. The alteration zone is wider near foliation planes, and narrower in more massive portions of the rock. With increasing distance from the quartz veins, the armenite crystals become smaller and more subhedral; moreover, both the number and the size of mineral inclusions in armenite increase. These inclusions were identified as zoisite, celsian, margarite, quartz and Ba-rich white mica or ganterite, and their chemical composition is identical to that of the same minerals found as rock-forming phases outside the zone of alteration (Tables 2–4). Both types of armenite have nearly ideal end-member composition (Table 5).

Table 5 Representative electron micoprobe analyses (in wt%) and stoichiometry of armenite from the Berisal Complex.

	Armenite				
Sample	SS9793N2*	SS9793N3	SS9854/1A	SS9854/3A	SS9854/4C
Distance from vein	0 cm	1–2 cm	10 cm	25 cm	40–45 cm
BaO	13.8	13.7	13.0	13.3	13.7
K_2O	0.03	0.04	0.04	0.01	<0.01
MgO	<0.03	<0.03	<0.03	<0.03	<0.03
Al_2O_3	27.6	27.3	26.9	27.2	27.0
SiO_2	48.3	48.8	46.7	46.9	47.7
FeO	<0.39	<0.39	0.03	<0.39	0.05
CaO	9.46	9.41	9.49	9.50	9.78
Na_2O	0.08	0.14	0.05	0.04	0.04
TiO_2	<0.15	<0.15	0.03	<0.15	0.13
MnO	<0.18	<0.18	0.10	0.19	0.02
Total	99.3	99.4	96.4	97.2	98.4
Stoichiometry based on 30 oxygens					
Ba	1.01	0.99	0.98	1.00	1.01
K	0.01	0.01	0.01	0.00	0.00
Sum	1.02	1.00	0.99	1.00	1.01
Ca	1.89	1.87	1.95	1.94	1.98
Na	0.03	0.05	0.02	0.01	0.01
Mn	0.00	0.00	0.02	0.03	0.00
Sum	1.92	1.92	1.98	1.98	1.99
Al	6.06	5.97	6.08	6.11	6.00
Ti	0.00	0.00	0.00	0.00	0.02
Si	9.00	9.07	8.96	8.93	8.98
Sum	15.06	15.04	15.04	15.04	15.00
Σ Cations	17.99	17.97	18.01	18.02	18.00

* Euhedral armenite from the vein-gneiss interface

In contrast to armenite and its mineral inclusions, the white micas in the alteration zone are heterogeneous (Table 6), exhibiting chemical zoning with Ba-rich cores and K-enriched rims (Fig. 4C). This chemical heterogeneity is in marked contrast to the white micas occurring in the armenite-free rock outside the alteration zone. K-rich areas are also found close to the cleavage planes of the micas, indicating secondary alteration. The extent of this alteration increases in individual micas the closer they are to the vein-gneiss boundary.

4. Profiles across the alteration zone

The modal abundance of armenite in the alteration zone decreases from 80 Vol% to zero along strike away from the vein-gneiss interface (Fig. 5). This decrease is mirrored by increases in the abundances of celsian, zoisite, margarite, and quartz, whereby the modal concentration of Ba-rich white micas remains relatively constant. The most pronounced armenite mineralisation is in the 10–15 cm of gneiss closest to the quartz vein (Fig. 4B). Beyond this region, armenite only oc-

Table 6 Chemical composition (in wt%, determined by EPMA) of a zoned Ba-rich muscovite in armenite-bearing leucocratic gneiss, 20 cm from the vein-gneiss interface. Point numbers relate to Figure 4C.

Point	1	2	3	4	5
BaO	10.9	8.0	12.8	14.0	8.9
K_2O	6.23	6.96	4.66	4.59	6.66
MgO	1.23	1.50	1.18	1.20	0.66
Al_2O_3	35.2	34.2	34.8	34.9	36.4
SiO_2	39.8	41.3	38.5	37.8	40.5
FeO	1.15	1.16	1.16	1.26	0.83
CaO	0.02	0.01	0.01	0.01	0.27
Na_2O	0.9	1.02	1.5	1.13	1.06
TiO_2	0.54	1.00	0.39	0.78	0.39
MnO	0.12	0.18	0.06	<0.07	0.04
Total	96.0	95.3	95.1	95.7	95.6
Stoichiometry based on 22 oxygens					
Ba	0.61	0.44	0.73	0.80	0.49
K	1.13	1.25	0.86	0.85	1.19
Na	0.25	0.28	0.42	0.32	0.29
Ca	0.00	0.00	0.00	0.00	0.04
Mn	0.01	0.02	0.01	0.00	0.00
Ti	0.06	0.11	0.04	0.09	0.04
Mg	0.26	0.31	0.26	0.26	0.14
Fe	0.14	0.14	0.14	0.15	0.1
Al_{oct}	3.56	3.47	3.56	3.51	3.71
Al_{tet}	2.34	2.19	2.40	2.49	2.32
Si	5.66	5.81	5.60	5.51	5.68
Σ Cations	14.02	14.02	14.02	13.99	14.00

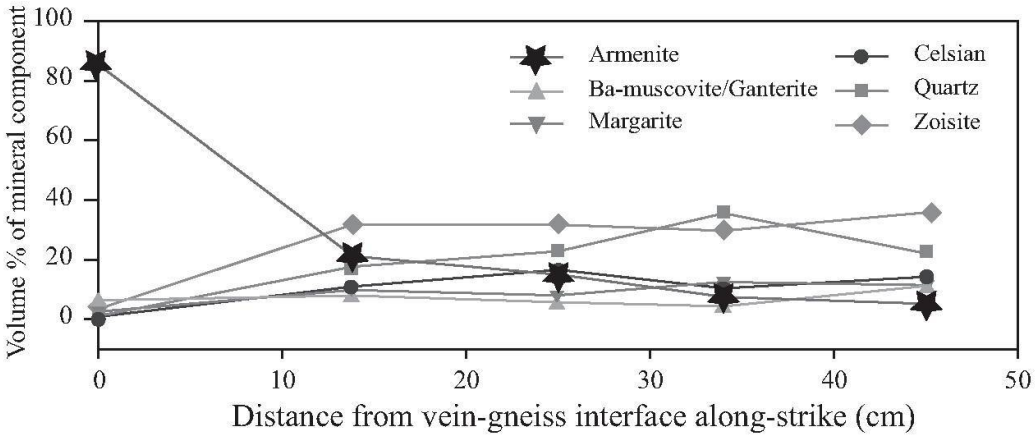

Fig. 5 Variation in modal abundance of different minerals along a profile through the zoisite-celsian gneiss, with increasing distance from the vein-gneiss interface.

curs along the grain boundaries of the other rock-forming minerals (Fig. 4D).

Considerable variation in the bulk chemical composition of the gneiss with distance from the vein is also observed. The distinct increase in armenite content is associated with an increase in the concentrations of BaO and SrO, and a decrease of the SiO_2 content (Fig. 6; Table 7). The concentrations of Al_2O_3 and CaO, on the other hand, remain fairly constant. Where armenite is less abundant, i.e., beyond 15–20 cm from the interface, the concentrations of all components remain relatively constant (Fig. 6).

To evaluate these chemical variations, an isocon diagram (Grant, 1986) was constructed (Fig. 7), which presents the relevant concentrations at four points along a profile. The two isocons shown were forced through the origin: the first assumes immobility of Al_2O_3, whereas the second assumes constant volume (constructed from the measured

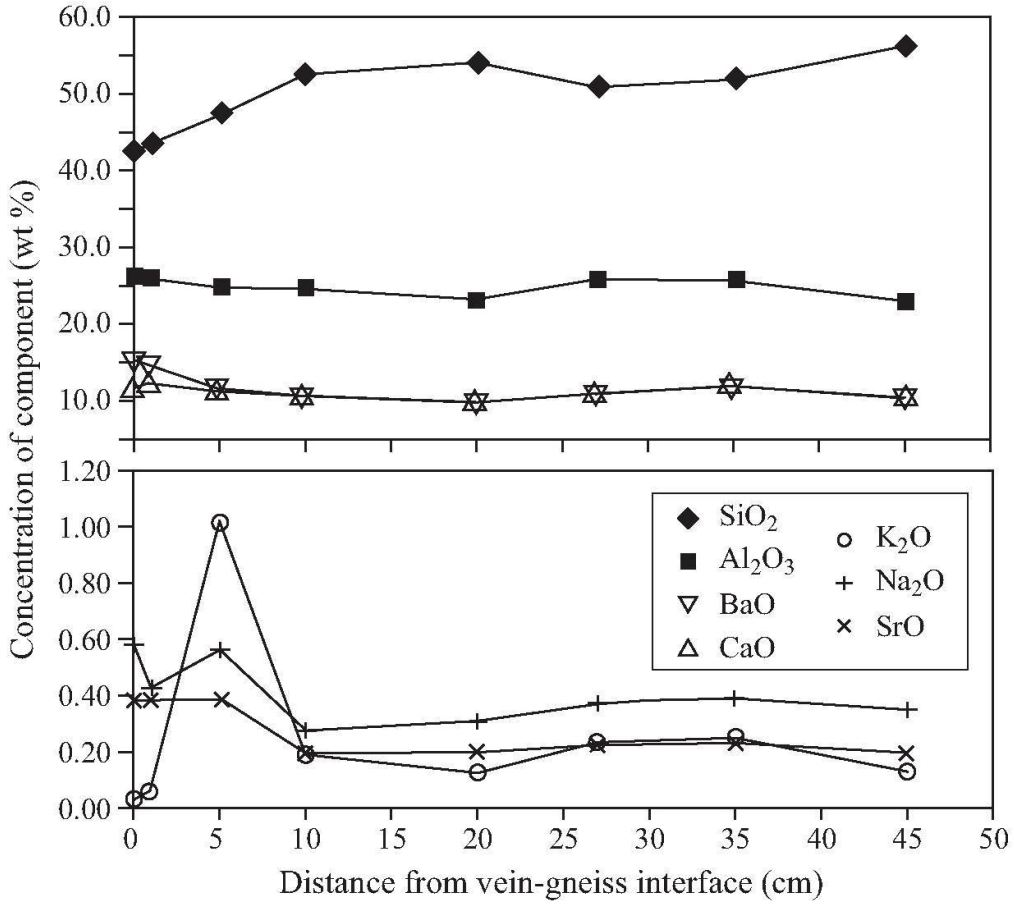

Fig. 6 Variation in whole-rock composition of the gneiss along the studied profile.

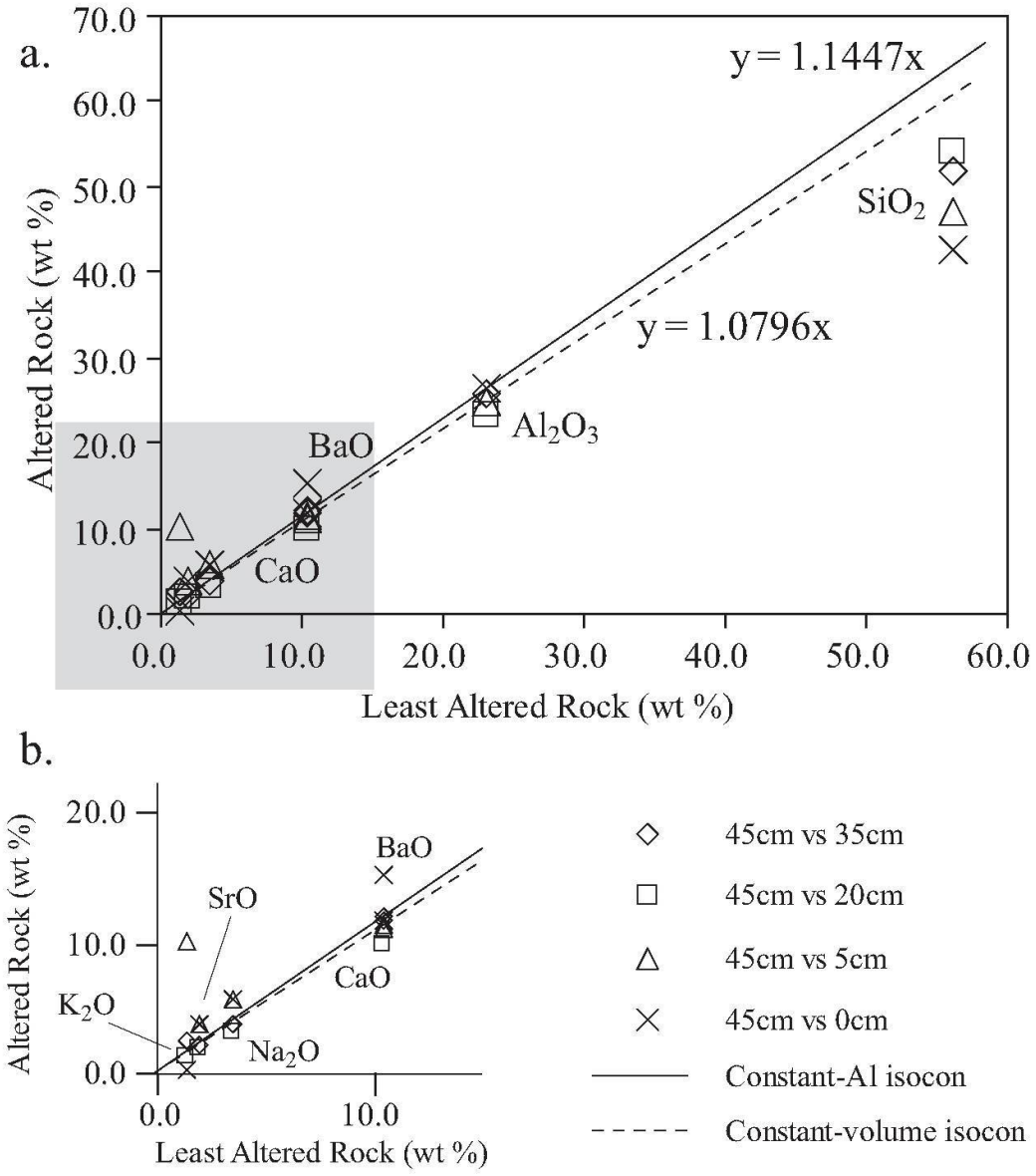

Fig. 7 Isocon diagram, with detail inset, for 4 samples of zoisite-celsian ± armenite gneiss (K_2O, Na_2O and SrO concentrations multiplied by 10).

density of each sample; see Table 7). There is no marked difference between the two isocons and, since there is no evidence for immobility of Al_2O_3, the following calculations are based on the constant-volume isocon. In accordance with Grant (1986), all points that lie above the isocon indicate a gain in that component, and all points lying below the isocon indicate a loss. All points lying on the isocon indicate that there has been no change in the relative concentration of that species. From Figure 7 it is clear that SiO_2 has been removed from the system, and that the quantity of SiO_2 being removed increases towards the vein, where the degree of alteration is greatest. For the zone closest to the vein, up to 30% of the original SiO_2 has been removed. The distribution of Al_2O_3, BaO, CaO, SrO and Na_2O shows a consistent pattern: at points furthest from the vein-gneiss interface the data plot on, or slightly below the constant-volume isocon. In contrast, closer to the veins, where the concentrations of armenite are greatest, the data plot above the isocon, thus indicating a slight enrichment in these components.

5. Characterisation of fluid-inclusion assemblages

Thin and thick sections have been prepared for rocks collected along profiles from the quartz veins, across the vein-gneiss interface, and along strike into the leucocratic gneiss. Each of the studied profiles covers a distance of approximately 50 cm. The most important observations were made in vein quartz, euhedral armenite, and in the 3–5 cm of gneiss closest to the vein-gneiss interface.

Table 7 Bulk composition (in wt%) and measured density (in g cm^{-3}) of leucocratic zoisite-celsian±armenite gneiss. Data shown for samples collected along a profile from the vein-gneiss interface (distance = 0 cm) into the gneiss at the studied outcrop.

Distance (cm)	Al_2O_3	SiO_2	CaO	SrO	BaO	K_2O	Na_2O	Density*
0	26.34	42.55	11.70	0.38	15.32	0.03	0.58	2.79
1	25.89	43.45	12.30	0.38	14.67	0.07	0.43	n.a.
5	24.76	47.23	11.23	0.39	11.50	1.02	0.56	2.89
10	24.58	52.56	10.64	0.20	10.70	0.19	0.28	2.96
20	23.23	54.09	9.80	0.20	9.82	0.13	0.31	2.95
27	25.85	50.88	10.94	0.22	10.90	0.24	0.37	2.90
35	25.66	51.86	12.04	0.23	11.90	0.25	0.39	2.92
45	23.01	56.23	10.46	0.20	10.40	0.13	0.35	3.01

* Density was measured using an evacuated representative specimen and Archimedes' principle. n.a. not analysed.

At least eight petrographic events could be distinguished in the evolution of the quartz veins and the crystallisation of armenite; four are directly related to fracture events (FE). Eight distinct fluid-inclusion assemblages have been identified and characterised (Table 8), and each one may be correlated with a specific event in the sequence of fracturing and mineralisation.

Event 1: The oldest recorded event after the brittle-ductile transition was initial fracturing and cleft formation (FE1). Vein quartz is the earliest observed phase in these fractures and contains at least two assemblages of fluid inclusions (1a, 1b; *Events 2 and 3*). These inclusions are typically ⩾40 μm and well formed (Fig. 8A), are either dispersed or arranged along short trails, and look like early secondary-type inclusions (showing negative quartz forms). They contain CO_2-enriched fluids (CO_2 liquid and vapour) of very low salinity. At room temperature, the 1a-inclusions have a large gas bubble (up to 50 Vol% of the inclusion), whereas those of the slightly younger 1b-assemblage have a smaller bubble (~35 Vol%). Assemblages 1a and 1b contain 24.1 and 14.1 mol% CO_2, respectively, and homogenise to a liquid or a vapour phase at 293 and 289 °C (Table 8). Melting of CO_2 in assemblage 1a occurs between –57.2 and –56.6 °C, indicating that the CO_2 is not pure, but that it contains a very small amount of other volatile species. Melting of CO_2 in assemblage 1b occurs at –56.6 °C, pointing to pure CO_2 gas. Clathrate in these two types of fluid inclusions dissociates between 8.8 and 8.9 °C, indicating that the amount of dissolved salts, as NaCl-equivalence, is around 0.6 mol%. This value is slightly under-estimated for the 1a-type, as the CO_2 contains other volatiles.

Event 4 fractured the vein-fill quartz close to the periphery of the veins (FE2). No fluid inclusions are found directly within the fracture planes, but the fracture-related fluid inclusions in vein-fill quartz (assemblage 2) have been identified in close proximity to the fractures. Ice melts at –3.9 °C, yielding a bulk salinity of 2.0 mol%. These inclusions homogenise to a liquid phase at 262 °C. No phase transitions are observed which would help to identify the volatiles present. Thus the fluid composition is classified as an aqueous chloride solution containing only a water-vapour bubble.

Event 5 is characterised by the petrographically oldest crystals of armenite. These armenites (A1) overgrow the quartz that was cracked during FE2, and are oriented with their c-axis parallel to the foliation and thus, perpendicular to the vein-gneiss interface. The A1-crystals host distinct fluid inclusions (assemblage 3), which are elongated, approximately 10–15 μm across, and aligned parallel to the c-axis of armenite (Fig. 8B). A first melting temperature of ~ –6.1 °C has been recorded for these inclusions, indicating the presence of electrolytes in the aqueous fluid. The average melting temperature of ice converts to a salinity of 2.8 mol% NaCl-equivalence. The clathrate dissociation temperature implies an approximate CO_2 content of 1.7 mol%.

Event 6 is a further period of fracturing, as evidenced in the gneiss (within 1.5 cm of the vein). It is seen petrographically in armenite-1, which has been fractured at least twice (FE3, FE4) and contains clearly definable trails of fluid inclusions. These inclusion trails may be traced over several mm, running parallel to the vein-gneiss interface, in a vertical manner, and perpendicular to the foliation (Fig. 8C). Two fluid-inclusion assemblages (4a, 4b) have been recognised, and are referred to as "armenite shear trails" (ASa, ASb). The inclusions measure approximately 25–30 μm in length and have similar bubble sizes (6–7 Vol%; Fig. 8D). The fluid inclusions homogenise to a liquid phase at approximately 169 and 157 °C, and are both water-rich (Table 8). Assemblage 4a has a higher ice-melting temperature than 4b, reflecting a lower salt content (1.0 vs. 2.3 mol%). No features were observed indicating a volatile phase, but the

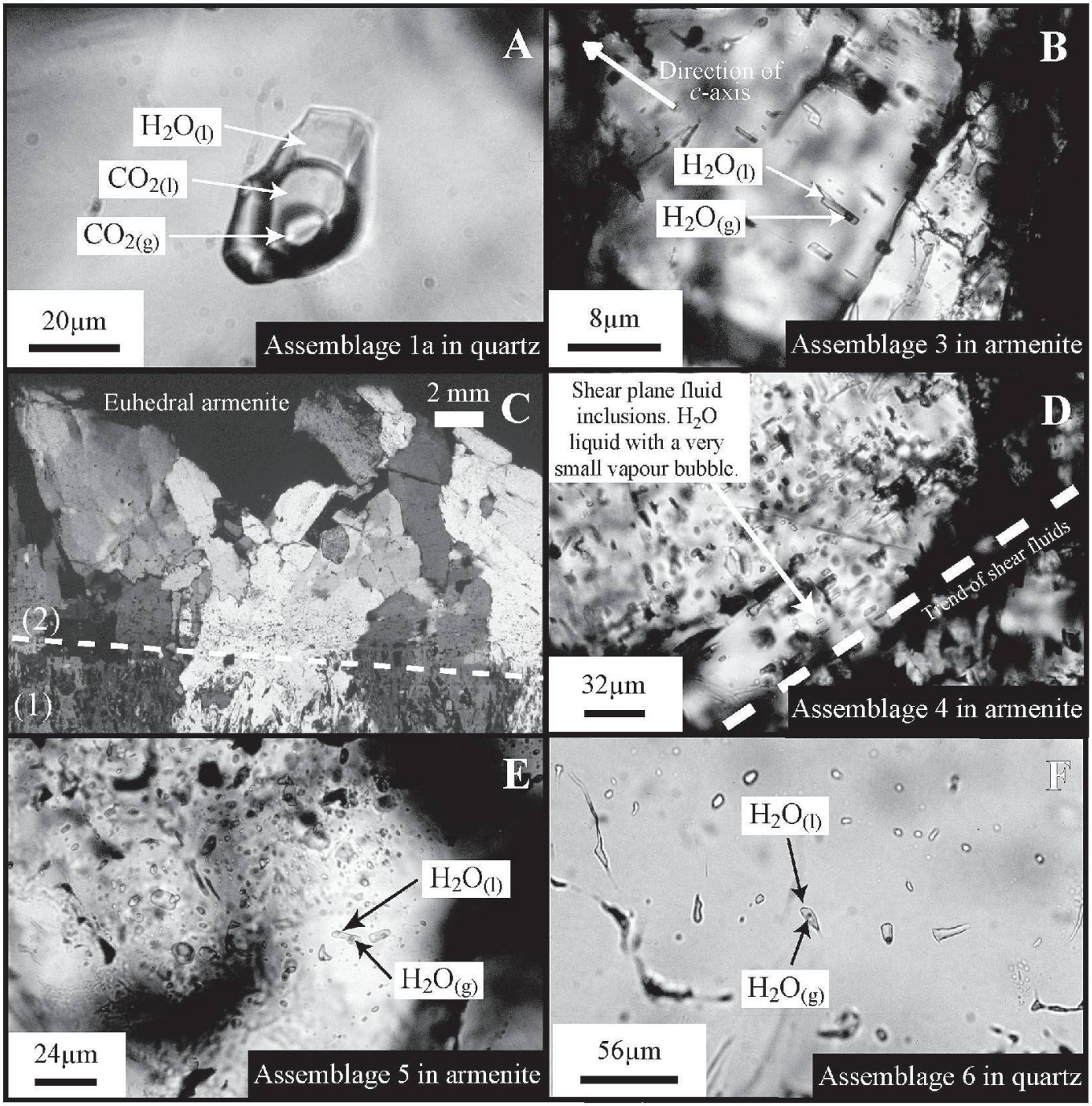

Fig. 8 Photomicrographs of important fluid-inclusion assemblages. (A) Single CO_2-rich fluid inclusion from assemblage 1a in vein-fill quartz. (B) Salt-enriched, CO_2-poor fluid inclusions from assemblage 3 in rock-forming armenite. (C) Interface of armenite-bearing gneiss and quartz veins: (1) armenite-1 in gneiss overgrown by euhedral armenite-2; and (2) boundary depicted by trails of shear-related fluid-inclusion assemblages parallel to the dashed line. (D) CO_2-poor fluid inclusions in assemblages 4a and 4b along a shear plane in armenite-1. (E) Salt-enriched, CO_2-poor fluid inclusions from assemblage 5 in euhedral armenite. (F) CO_2-free, aqueous chloride-bearing fluid inclusions from assemblage 6 in late vein-fill quartz.

clathrate dissociation temperatures point to the presence of some CO_2 (1.9 and 1.7 mol%, respectively).

Event 7: Overgrowing the youngest fractures in A1-armenite are euhedral armenite crystals. The best examples are at the vein-gneiss interface, but good material was also found in cavities in the zoisite-celsian host rock very close to the veins (2–3 cm). This second generation of armenite (A2) contains distinct fluid inclusions (assemblage 5), which are all of similar size (~5–15 μm), have an estimated bubble size of 5.5 Vol%, and are randomly oriented (Fig. 8E). Microthermometric and compositional data for these inclusions are nearly identical to those observed for inclusions in the older A1-crystals. They also homogenise to a liquid phase, but at lower temperatures (around 153 °C).

Event 8: The final fluid-inclusion type (assemblage 6) postdates all armenite growth, and is most easily recognised in vein-fill quartz. These inclusions are generally similar in size (<15 μm), shape (Fig. 8F) and composition, containing a very small bubble (3.5 Vol%). Initial freezing occurs at –54 °C, suggesting that, in addition to NaCl, other salts are present in the aqueous solution. Ice melting at –2.7 °C implies a salinity of 1.4 mol% NaCl equivalence. These inclusions homogenise to a liquid at 130 °C.

6. Evolution of P, T and fluid composition

From estimated bubble size and fluid composition, the total density of each fluid-inclusion assemblage has been calculated, and isochores were constructed, using the equation of state of the ternary system H_2O–CO_2–NaCl after Bowers and Helgeson (1983). These isochores are displayed in Fig. 9, which also shows an average geothermal gradient of 30 °C/km for the Central Alps (Wagner et al., 1977) at corresponding fluid pressures for hydrostatic ($P_{hydrost}$) and lithostatic (P_{lith}) conditions. The fluid pressure can be reconstructed for each fluid-inclusion assemblage from the intersection of its formation temperature with the corresponding isochore. Where formation temperature is not known, the formation pressure can be estimated from the intersection of the lithostatic geothermal gradient with the isochores of the different fluid assemblages. This procedure yields a good approximation, as retrograde fluid pressures in a metamorphic belt are close to P_{lith} (Mullis et al., 1994).

During uplift and fracturing of the leucocratic gneiss, the equilibrium between the fluid pressure and P_{lith} was disturbed. CO_2-enriched, salt-poor fluids moved into the clefts where the solubility of SiO_2 in the fluid decreased, resulting in quartz precipitation. This vein-filling quartz entrapped fluid-inclusion assemblages 1a and 1b.

Assemblages 1a and 1b: based on the formation temperatures of quartz veins at localities with similar fluid composition from the Central Alps (Mullis et al., 1994; Mullis, 1996), the formation temperatures for these CO_2-enriched fluids were estimated at 450–420 °C, yielding a formation pressure around 3 kbar, i.e. close to P_{lith}. The fluid composition is interesting because there is no obvious source of CO_2 in the immediate vicinity of the veins. However, early CO_2-rich fluids are reported from many localities and varying rock types across the Central Alps (Mullis et al., 1994), and the occurrence of CO_2-rich fluids in calcite-free crystalline rocks is not unique.

Assemblage 2: these fluids with a considerably lower density than the earlier fluids were entrapped at ~350 °C and 1.1 kbar, as deduced from the intersection of their isochore with the hydrostatic geotherm. Their composition is markedly

Table 8 Characteristics of the observed fluid-inclusion assemblages.

1 FIA	2 HM	3 IT	4 nI	5 VoT	6 V%	7 Tm_{ice}	8 Tm_{CO2}	9 Td_{Cl}	10 Th_{CO2}	11 ThI	12 H_2O mol%	13 CO_2 mol%	14 NaCl mol%	15 NaCl wt%	16 D.M.
1a	VFQ	II	9	CO_2	50 ± 5	n.m.	–57.2	8.8	25.5L	293/289–297V	75.3	24.1	0.6	2.4	Rt, A
1b	VFQ	II	23	CO_2	35 ± 5	n.m.	–56.6	8.9	29.5L	289/288–292L	85.5	14.1	0.6	2.2	Rt, A
2	VFQ	II	18	n.o.	15–20	–3.9/–3.8–4.0	n.o.	n.o.	n.o.	262/259–265L	>97.00	<1.0	2.0	6.2	A
3	A 1	II	14	CO_2	7 ± 1	–5.6/–5.0–6.1	n.o.	3 / 2–4	n.o.	212/206–217L	95.5	1.7	2.8	8.8	A
4a	AS*a*	II	6	CO_2	6.5	–1.9/–1.8–2.2	n.o.	5 / 5–6	n.o.	169/166–176L	97.1	1.9	1.0	3.2	A
4b	AS*b*	II	13	CO_2	6	–4.6/–4.2–5.4	n.o.	3 / 3–4	n.o.	157/140–181L	96.0	1.7	2.3	7.2	A
5	A 2	II	16	CO_2	5.5	–5.5/–5.0–5.8	n.o.	4 / 4–5	n.o.	153/135–174L	95.4	1.9	2.7	8.5	A
6	VFQ	II	10	n.o.	3.5	–2.7/–2.4–3.0	n.o.	n.o.	n.o.	130/125–136L	>97.6	<1.0	1.4	4.5	A

Notes:
(1) FIA — Fluid inclusion assemblage. (2) HM — Host mineral: VFQ — Vein-fill quartz; A1 — rock-forming armenite; A2 — Euhedral armenite; AS — Sheared armenite. (3) IT — Inclusion Type: II — Secondary fluid inclusions. (4) nI — Number of measured fluid inclusions. (5) VoT — Volatile type. (6) V% — Volume-% of the volatile part estimated at room temperature. (7) Tm_{ice} — Melting temperature of ice (°C). First number — mean value; second and third number — extreme values (range); n.m. — not measured. (8) Tm_{CO2} — Melting temperature of solid CO_2 (°C); n.o. — not observed. (9) Td_{Cl} — Dissociation temperature of clathrate (°C). First number — mean value; second and third number — extreme values (range); n.o. — not observed. (10) Th_{CO2} — Homogenisation temperature of CO_2. L — homogenisation to the liquid phase. (11) ThI — Homogenisation temperature of fluid inclusions. L — homogenisation to the liquid phase; V — homogenisation to the vapour phase. First number — mean value; second and third number — extreme values (range). (12–14) Approximate mol% of H_2O, CO_2 and $NaCl_{equivalence}$. (15) Approximate wt% of $NaCl_{equivalence}$. (16) D.M. — daughter minerals. A — anisotropic solid; Rt — Rutile.

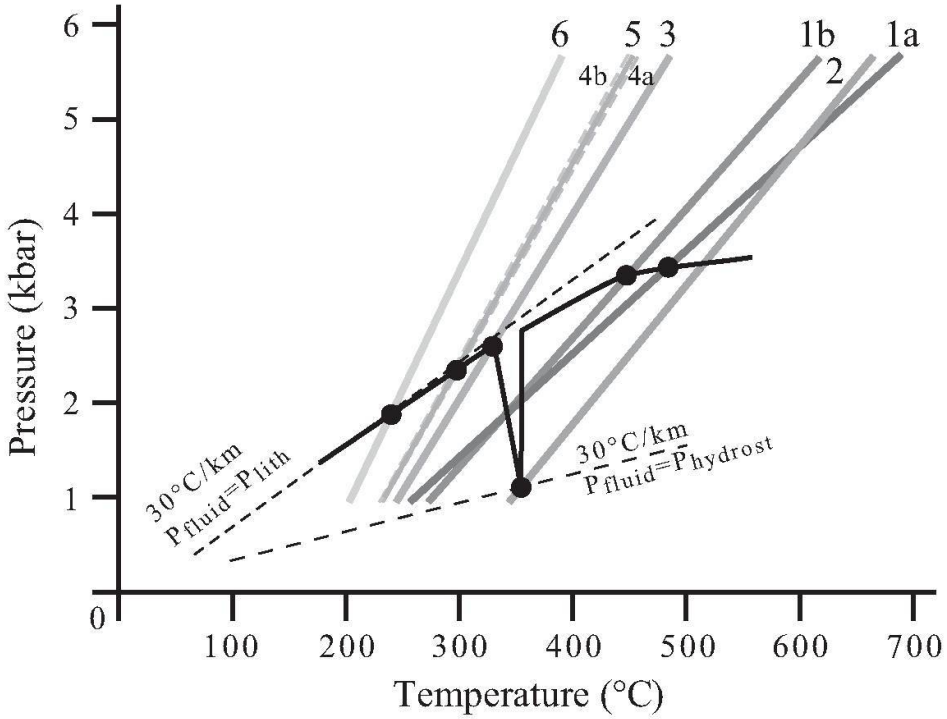

Fig. 9 Fluid P–T diagram for the studied fluid-inclusion assemblages. Each numbered isochore corresponds to a single fluid-inclusion assemblage (Table 8).

different from that of the earlier fluids (Table 8). The elevated salt content (Fig. 10) suggests that it may have originated from a different source area and possibly passed through evaporite-type rocks (e.g., Mesozoic metasediments between the crystalline basement nappes). The absence of CO_2 indicates that there has been little mixing with earlier fluids.

Assemblage 3: its isochore intersects with the geothermal gradient of 30 °C/km ($P_{fluid} \approx P_{lith}$) at 325 °C and 2.6 kbar, suggesting that armenite first formed at these conditions. The even higher salt content of fuid-inclusion assemblage 3 (Fig. 10) indicates a direct relationship with fluid 2. However, it contains some CO_2 suggesting mixing with the original CO_2-bearing local fluid (Fig. 11).

Assemblages 4a, 4b and 5: the isochores of these fluids intersect the same geothermal gradient at approximately 295 °C and 2.3 kbar. It is at these conditions that the A1-crystals were fractured and the euhedral second generation of armenite began to grow. Fluid-inclusion assemblage 4a contains less salt than assemblages 2 and 3, but slightly more CO_2 than assemblage 3. The lack of evidence for the influx of an external fluid indicates that mixing of two local fluids (e.g., 1 and 3) is a likely means of generating this fluid (Fig. 11). The linear distribution of fluid-inclusion assemblage 4a is interpreted as showing that their entrapment was the result of limited recrystallisation of armenite in response to localised strain. The 4b-inclusions are much more abundant than those of assemblage 4a, and they are associated with fracturing of armenite, indicating that the intensity of strain was increasing. This culminated with the clefts being flushed by fluid 5, which is similar in composition to fluid 3. The movement of fluid 5 into the system is contemporaneous with crystallisation of A2-armenite at the interface between the gneiss and the quartz vein.

Assemblage 6: the intersection between isochore and geothermal gradient is below 250 °C and 2 kbar. These fluid inclusions represent the final stages of mineral formation in the Alpine veins studied. There is no petrographic evidence that may be used to constrain a single event with regard to entrapment or evolution of fluid-inclusion assemblage 6 in quartz.

7. Discussion of armenite growth

The existence of at least two localities of zoisite-celsian gneiss in the Berisal Complex, but the presence of armenite only at the one cut by late Alpine veins highlights the importance of hydrothermal activity in the formation of the rare Ba-silicate. The systematic change in mineralogical and chemical composition of the rock with distance to the vein, puts further emphasis on the importance of hydrothermal fluids and associated metasomatic effects.

The presence of syn-kinematic Ba-silicates of relatively constant chemical composition in both

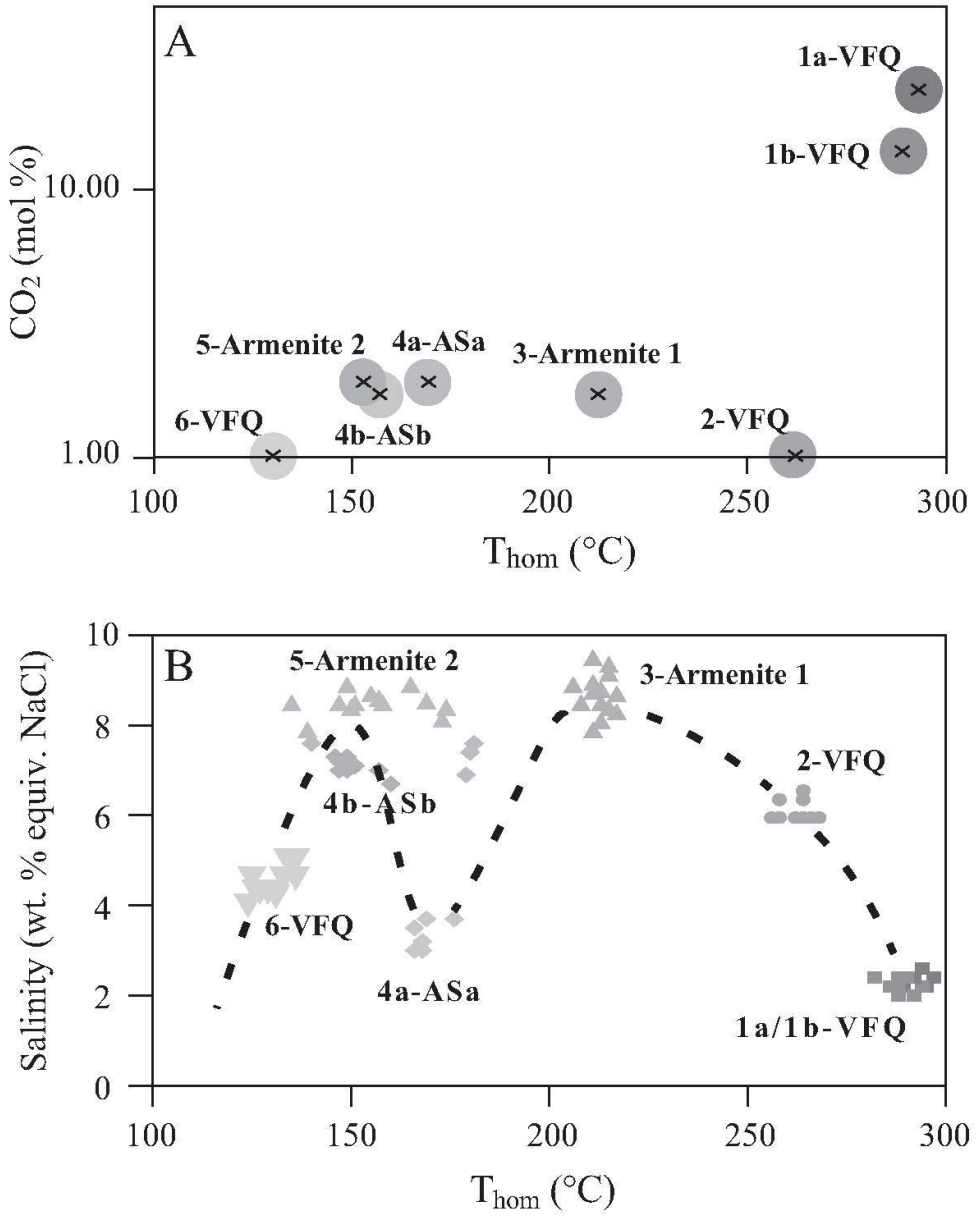

Fig. 10 (A) CO_2 content *vs.* T_{hom} and (B) Salinity *vs.* T_{hom} for fluid-inclusion assemblages. VFQ—vein-fill quartz.

altered and unaltered zoisite-celsian gneiss (Tables 2–4), suggests that much of the Ba was present in the gneiss prior to vein formation and hence, that armenite grew by *in-situ* recrystallisation of the Alpine metamorphic assemblage, probably via a reaction that consumed zoisite, celsian, margarite, and quartz.

The relatively constant modal abundance of Ba-rich white mica in the alteration zone indicates that this mica only played a limited role in the reaction *per se*; however, the chemical zoning of micas within the alteration zone suggests that they may have contributed some Ba to the process, which in turn means that some K must have been introduced to the system.

The significant variation in the concentration of SiO_2 in the alteration zone adjacent to the veins reflects dissolution of quartz and transport of SiO_2 from the gneiss into the veins where quartz precipitated during the first stages of late Alpine extension and fracturing. The bulk-rock contents of the other major species increases slightly, probably representing a relative enrichment due to the removal of SiO_2 (Fig. 7). The short-range transport of SiO_2 from the wall rock into the veins and the lack of evidence that chemical components were introduced into the system suggest that the earliest CO_2-enriched, low-salinity fluids (1a, 1b) may have evolved from devolatilisation reactions during Alpine metamorphism of gneiss and nearby sedimentary units.

The fracturing of vein-fill quartz resulted in a decrease of both fluid density and pressure (by ~1.7 kbar), which reduced the fluid pressure from P_{lith} to $P_{hydrost}$ (Fig. 9). A similar pressure drop has been documented in a *Bündnerschiefer*-hosted Alpine fissure, occurring between the Berisal Complex and Monte Leone Nappe in the nearby

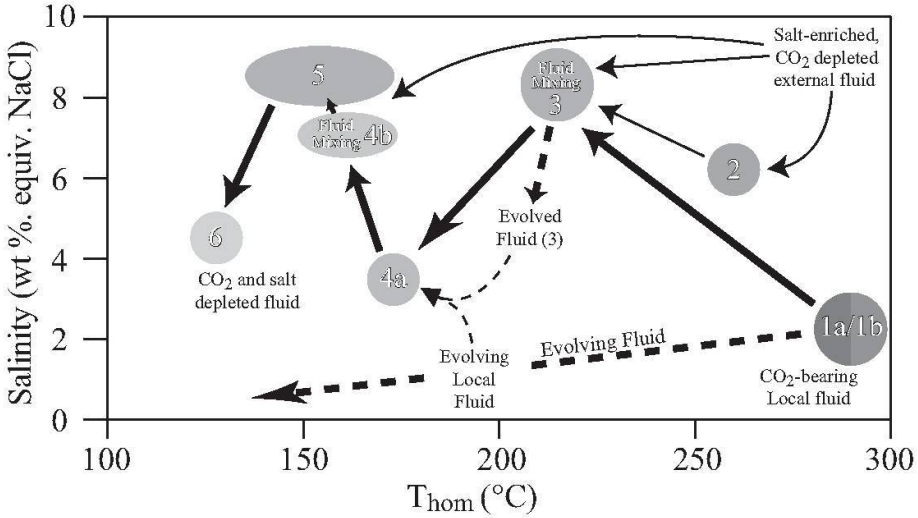

Fig. 11 Schematic representation and interpretation of events related to armenite formation in the Berisal Complex.

Steinental (Mullis 1983), indicating that such depressurisation was regionally widespread.

Re-establishment of $P_{fluid} = P_{lith}$ is coeval with the growth of armenite-1 and a change in the composition of the entrapped fluid inclusions. This first generation of armenite grew in the alteration zone adjacent to the veins and in cavities formed by the earlier removal of quartz. Therefore, we assume that there was some fluid percolation along the foliation planes into the gneiss, inducing the armenite-forming reaction. Here, the salt-enriched fluid was mixed with the evolving retrograde CO_2-bearing local fluid (Fig. 11). The zoned micas indicate that the salt was not a pure Na-salt, but must have contained some K.

After this re-equilibration of P_{fluid}, the gneiss was uplifted and cooled, and the armenite-1 crystals were strained, as evidenced by fluid-inclusion trails parallel to shear planes. The increase in strain is recorded by trapping of salt- and CO_2-depleted fluids. When the strain reached a critical point, armenite-1 was fractured. The fractures are overgrown by a second generation of armenite (A2), which entrapped a more saline fluid similar in composition to that responsible for crystallisation of armenite-1. This additional input of salt-enriched fluids promoted crystallisation of armenite-2, which is euhedral and occurs at the edges of the Alpine fissures and cavities, but not in the gneiss.

8. Conclusions

From the microtextural evidence found in the zoisite-celsian gneiss we conclude that armenite crystallised as the result of a reaction between zoisite, celsian, margarite, and quartz. The reaction took place close to the vein-gneiss interface and was promoted by infiltration of water- and salt-rich, CO_2-depleted fluids that mixed with evolving retrograde CO_2-bearing fluids. The influx of fluids was driven by fracturing and reduction in P_{fluid}.

Crystallisation of armenite in the Berisal Complex was a hydrothermally driven process, which occurred on the retrograde path of Alpine metamorphism, most probably at temperatures of 320–280 °C and pressures between 2.6 and 2.0 kbar. Percolation and mixing of the fluids was promoted by earlier removal of rock-forming quartz, which was transported into, and precipitated in, the Alpine clefts in the form of vein-fill quartz. This led to increased permeability and cavities in the wall rock, which were subsequently filled by armenite. Brittle deformation of the Berisal Complex was tectonically controlled during uplift of the Western Lepontine Dome and extension on the Simplon Fault Zone.

Acknowledgements

Research was supported by grants 20-46906.96 and 20-46906.00 from the Swiss National Research Foundation. CJH acknowledges personal funding from the Freiwillige Akademische Gesellschaft in Basel. Martin Engi and an anonymous reviewer are thanked for helpful reviews of an earlier version of this manuscript.

References

Angus, S., Armstrong, B., De Reuk, K.M., Altunin, V.V., Gadetskil, O.G., Chapala, G.A. and Rowlinson, J.S. (1973): International thermodynamic tables of the fluid state: Carbon dioxide. International Union of Pure and Applied Chemistry, Pergamon.

Balassone, G., Boni, M., Di Maio, G., and Franco, E. (1989): Armenite in southwest Sardinia: first recorded occurrence in Italy. *N. Jb. Mineral. Mh.* **2**, 49–58.

Bowers, T.S. and Helgeson, H.C. (1983): Calculation of the thermodynamic and geochemical consequences of non ideal mixing in the system H_2O–CO_2–NaCl on phase relations in geologic systems. Equation of state for H_2O–CO_2–NaCl fluids at high pressures and temperatures. *Geochim. Cosmochim. Acta.* **47**, 1247–1275.

Bozzo, A.T., Chen, H-S., Kass, J.R. and Barduhn, A.J. (1973): The properties of the hydrates of chlorine and carbon dioxide. In: Dekyannis, A. and Delyannis, E. (eds): The Fourth International Symposium on Fresh Water from the sea. Vol 3, pp. 437–451.

Chen, H-S. (1972): The thermodynamics and composition of carbon dioxide hydrate. M.Sc. thesis, Syracuse University.

Diamond, L.W. (1992): Stability of CO_2 clathrate hydrate + CO_2 liquid + CO_2 vapour + aqueous KCl–NaCl solutions: Experimental determination and application to salinity estimates of fluid inclusions. *Geochim. Cosmochim. Acta.* **56**, 273–280.

Diamond, L.W. (1994): Salinity of multi-volatile fluid inclusions determined from clathrate hydrate stability. *Geochim. Cosmochim. Acta.* **58**, 19–41.

Drummond, S.E. (1981): Boiling and mixing of hydrothermal fluids: chemical effects on mineral precipitation. Ph.D. thesis, Pennsylvania State University.

Forbes, W.C., Baur, W.H. and Khan, A.A. (1972): Crystal chemistry of milarite-type minerals. *Am. Mineral.* **57**, 463–472.

Forfey, N.J., Nancarrow, P.H.A. and Gallagher, M.J. (1991): Armenite from the Middle Dalradian of Scotland. *Mineral Mag.* **55**, 135–138.

Frank, E. (1983): Alpine metamorphism of calcareous rocks along a cross-section in the Central Alps: occurence and breakdown of muscovite, margarite and paragonite. *Schweiz. Mineral. Petrogr. Mitt.* **63**, 37–93.

Graeser, S. (1993): Armenit vom Simplon – ein sensationeller Neufund. *Mineralien Welt*, **6**, 39–43.

Graeser, S., Hetherington, C.J. and Gieré, R. (2003): Ganterite, a new barium-dominant analogue of muscovite from the Berisal Complex, Simplon Region, Switzerland. *Can. Mineral.* **41**, 1271–1280.

Grant, J.A. (1986): The isocon diagram – A simple solution to Gresens' equation for metasomatic alteration. *Econ. Geol.* **81**, 1976–1982.

Hetherington, C.J. (2001): Barium anomalies in the Berisal Complex, Simplon Region, Switzerland. Ph.D. thesis, University of Basel.

Hetherington, C.J., Mullis, J., Gieré, R. and Graeser, S. (2001): Armenite formation in the Berisal Complex, Simplon, Switzerland. *J. Conf. Abs.* **6(1)**, 575.

Hetherington, C.J., Gieré, R. and Graeser, S. (2003): Composition of barium-rich white micas from the Berisal Complex, Simplon Region, Switzerland. *Can. Mineral.* **41**, 1281–1291.

Heyen, G. Ramboz, C. and Dubessy, J. (1982): Simulation des équilibres de phases dans le système CO_2–CH_4 en dessous de 50 °C et de 100 bars. *C.R. Acad. Paris Sér.* **294**, 203–206.

Köhn, M. (1993): Barium-Anomalien im Grenzbereich Monte Leone-Decke/Berisalserie, Bortelhorn (VS). Diploma thesis, University of Basel.

Kretz, R. (1983): Symbols for rock-forming minerals. *Am. Mineral.* **68**, 277–279.

Mancktelow, N.S. (1990): The Simplon Fault Zone. *Beitr. Geol. Karte Schweiz* **163**, 66 pp.

Mason, B. (1987): Armenite from Broken Hill, Australia, with comments on calciocelsian and barium anorthite. *Mineral. Mag.* **51**, 317–318.

Merle, O., Cobbold, P.R. and Schmid, S. (1989): Tertiary kinematics on the Lepontine dome. In: Coward, M.P., Dietrich, D. and Park, R.G. (Eds): *Alpine Tectonics.* Geological Society Spec. Publ. **45**, p. 113–134.

Mullis, J. (1983): Einschlüsse in Quarzkristallen der Schweizer Alpen und ihre mineralogisch-geologische Bedeutung. *Bull. Soc. Fribourg. Sc. Nat.* **72**, 5–19.

Mullis, J., Dubessy, J., Poty, B. and O'Neil, J. (1994): Fluid regimes during late stages of a continental collision: Physical, chemical, and stable isotope measurements of fluid inclusions in fissure quartz from a geotraverse through the Central Alps, Switzerland. *Geochim. Cosmochim. Acta.* **58**, 2239–2267.

Mullis, J. (1996): P–T–t path of quartz formation in extensional veins of the Central Alps. *Schweiz. Mineral. Petrogr. Mitt.* **76**, 159–164.

Neumann, H. (1939): Armenite, a new mineral. Preliminary note. *Norsk Geologisk Tidsskrift* **19**, 312–313.

Potter, R.W., II Clynne, M.A. and Brown, D.L. (1978): Freezing point depression of aqueous sodium solutions. *Econ. Geol.* **73**, 284–285.

Poty, B., Leroy, J. and Jachimonicz, L. (1976): Un nouvel appareil pour le mesure des température sous le microscope: l'installation de microthermometrie Chaixmeca. *Bull. Minéral.* **99**, 182–186.

Pouliot, G., Trudel, P., Valiquette, G. and Samson, P. (1984): Armenite-thulite-albite veins at Rémigny, Quebec: The second occurrence of Armenite. *Can. Mineral.* **22**, 453–464.

Schwartz, M.O. (1989): Determining phase volumes of mixed CO_2–H_2O inclusions using microthermometric measurements. *Mineral. Deposita* **24**, 43–47.

Semenenko, N.P., Litvin, A.L., Sharkin, O.P., Boiko, V.L., Ergrova, L.N., Skuridin, G.S., Terets, G.S., Savitskaya, A.B. and Ilovayskaya, S.V. (1987): Armenite from the Middle Pridneprov'ya (USHCH) – first mentioned occurrence in the USSR. *Mineralogicheskiy Zhurnal* **9(6)**, 83–90.

Senn, T. (1989): Barium-Mineralisation und Barium-Gneise/Wasenalp (VS). Diploma thesis, University of Basel.

Steck, A. and Hunziker, J. (1994): The Tertiary structural and thermal evolution of the Central Alps-compressional and extensional structures in an orogenic belt. *Tectonophysics* **238**, 229–254.

Stille, P. (1980): On the genesis of the amphibolites and hornblende felses in the Berisal Complex (Simplon; Italy–Switzerland). *Mem. Ist. Geol. Padova* **34**, 205–246.

Taylor, S.R. and McLennan, S.M. (1981): The composition and evolution of the continental crust: rare earth element evidence from sedimentary rocks. *Phil. Trans. R. Soc. London* **A301**, 381–399.

Wagner, G.A., Reimer, G.M. and Jäger, E. (1977): Cooling ages derived by apatite fission-track, mica Rb–Sr and K–Ar dating: the uplift and cooling history of the Central Alps. *Mem. Ist. Geol. Padova* **30**, 1–28.

Zak, L. and Obst, P. (1989): Armenite-feldspar veins in basic volcanic rocks from Chvaletice (Czechoslovakia). *Casopis Pro Mineralogii A Geologii* **34(4)**, 337–351.

Zhang, Y.G. and Frantz, J.D. (1987): Determination of the homogenisation temperatures and densities of supercritical fluids in the system NaCl–KCl–$CaCl_2$–H_2O using synthetic fluid inclusions. *Chem. Geol.* **64**, 335–350.

Received 16 December 2002
Accepted in revised form 6 February 2004
Editorial handling: M. Engi